Disentangling changes in the river bed profile

The morphological impact of river interventions in a managed river

van Denderen, R. Pepijn; Kater, Emiel; Jans, Luc H.; Schielen, Ralph M.J.

DOI
10.1016/j.geomorph.2022.108244

Publication date
2022

Document Version
Final published version

Published in
Geomorphology

Citation (APA)
van Denderen, R. P., Kater, E., Jans, L. H., & Schielen, R. M. J. (2022). Disentangling changes in the river bed profile: The morphological impact of river interventions in a managed river. *Geomorphology*, *408*, Article 108244. https://doi.org/10.1016/j.geomorph.2022.108244

Geomorphology 408 (2022) 108244

Contents lists available at ScienceDirect

Geomorphology

journal homepage: www.journals.elsevier.com/geomorphology

Disentangling changes in the river bed profile: The morphological impact of river interventions in a managed river

R. Pepijn van Denderen [a,b,*], Emiel Kater [c], Luc H. Jans [c], Ralph M.J. Schielen [c,d]

[a] Marine and Fluvial Systems, Faculty of Engineering Technology, University of Twente, the Netherlands
[b] HKV, the Netherlands
[c] Ministry of Infrastructure and Water Management-Rijkswaterstaat, the Netherlands
[d] Faculty of Civil Engineering and Geosciences, Delft University of Technology, the Netherlands

ARTICLE INFO

Keywords:
River interventions
River bed level
Equilibrium
River engineering
River morphodynamics
Wavelet transform

ABSTRACT

The river bed level in low-land rivers like the Rhine branches in The Netherlands changes continuously on various spatial and temporal scales. Large-scale degradation occurs in many rivers due to river-wide engineering interventions, such as channelization, in the last decades and centuries. Local river interventions, such as the construction of side channels, affect the river's morphology by mainly causing sedimentation over the length of the intervention. This sedimentation occurs at a smaller spatial scale than the erosion due to channelization. On an even smaller spatial scale, dune-like bedforms migrate along the river bed but these have a net-zero effect on the morphology. This shows that bed-level changes occur on different spatial scales. Disentangling these spatial scales is appealing from a river management point of view since mitigating large-scale degradation requires a different river management strategy than mitigating erosion and sedimentation due to local interventions.

We use detailed bed-level measurements to study the morphological changes on multiple scales using a wavelet transform. A wavelet transform is, unlike a Fourier transform, able to distinguish and disentangle the bed-level changes on different spatial scales while taking into account its spatial variation. Using the wavelet transform, we can disentangle the bed level change caused by a local intervention from the large-scale bed degradation. Both bed level changes are in the same order of magnitude and thereby difficult to determine without filtering. This allows us to study the morphological changes resulting from a single river intervention. The results show that interventions such as side channels cause an average bed-level increase around which the bed level fluctuates. This dynamic component can be up to 6 times larger than the average change. The average bed level increase is in the same order of magnitude as analytical estimations for the equilibrium bed level change.

Disentangling spatial scales of bed level changes gives a better understanding of the impact of local interventions and past channelization. These insights can be used to optimize the operation and management of the river and thereby accommodate the main river functions.

1. Introduction

A river bed continuously changes at various spatial and temporal scales (Buffington, 2012; Church and Ferguson, 2015). Large-scale temporal and spatial bed-level changes are generally a result of changes in the occurrence and duration of high and low discharges over several years, the grain size-specific sediment flux or the base level (e.g., due to sea-level rise) (Gilbert, 1877; Mackin, 1948; Lane, 1955; Blom et al., 2017). In many rivers, large-scale human interventions in the last centuries are the most important cause of large-scale bed degradation (Habersack, 1996; Surian and Rinaldi, 2003; Hohensinner et al., 2004; Gregory, 2006; Sieben, 2009; Nittrouer and Viparelli, 2014; Havinga, 2020; Ylla Arbós et al., 2021). For the river Rhine, these interventions include channel straightening and narrowing over lengths of tens of kilometers (Ylla Arbós et al., 2021). These large-scale interventions are also known as the channelization and have been implemented in the river Rhine since the 17th-century (Van Til, 1979; Kalweit et al., 1993; Visser, 2000). The response of the river bed to large-scale channelization typically takes place over long timescales (decades to centuries) and large spatial scales (tens to hundreds of kilometers) (see Visser, 2000;

* Corresponding author at: Marine and Fluvial Systems, Faculty of Engineering Technology, University of Twente, the Netherlands.
E-mail address: p.vandenderen@hkv.nl (R.P. van Denderen).

https://doi.org/10.1016/j.geomorph.2022.108244
Received 5 February 2022; Received in revised form 3 April 2022; Accepted 3 April 2022
Available online 7 April 2022

Ten Brinke, 2005; Sieben, 2009; Church and Ferguson, 2015; Ylla Arbós et al., 2021). Locally, the bed level changes much faster and on a smaller spatial scale as a result of migrating bedforms, discharge fluctuations or interventions (e.g., Arkesteijn et al., 2019).

In this paper, we define three spatial scales of bed level changes: small, intermediate and large-scale bed level variations (Fig. 1). The *small spatial scale* of morphological changes (Fig. 1A) manifests in, for example, migrating bedforms like dunes that adapt over small temporal scales to new flow conditions (Julien et al., 2002; Wilbers and Ten Brinke, 2003). Also, local morphological effects of artificial groynes or other structures may cause small-scale morphological changes. These changes occur continuously and are independent of interventions (intermediate scale) or bed slope changes (large scale). The time-averaged bed level change resulting from these small-scale bed level variations is approximately zero, but the bed level variation is in the order of 0.5–1 m.

On an *intermediate spatial scale*, localized human interventions, such as the construction of side channels (Habersack and Nachtnebel, 2005; Van Denderen et al., 2019b) and longitudinal training dams (Havinga et al., 2009; De Ruijsscher et al., 2019), cause a local response of the riverbed. These interventions are constructed as part of river-restoration projects (Formann et al., 2007; Riquier et al., 2015; Wohl et al., 2015), to increase flood safety (Simons et al., 2001; Van Stokkom et al., 2005; Havinga, 2020) or to accommodate other river functions such as navigation (Havinga et al., 2009). Many interventions, such as side channels, withdraw discharge from the main channel to the floodplain and, thereby, reduce the sediment transport capacity in the main channel, increasing the main channel's bed level over the length of the intervention (Fig. 1B) (Habersack and Nachtnebel, 2005; De Vriend, 2015). The time scale over which the bed-level change occurs depends on the spatial scale of the intervention (typically in the order of kilometers) and is generally in the order of years. This is much faster than the large-scale response due to the large-scale channelization.

The bed-level change resulting from an intervention can be divided into an average and a dynamic response. The average response is constant in time and space and can be estimated using rules of thumb (Appendix A) based on equilibrium theory (Jansen et al., 1979; Blom et al., 2017). Theoretically, the average response will only be reached if the river is in a (quasi-)equilibrium state before and after the construction of the intervention (Jansen et al., 1979; De Vriend, 2015). Apart from this, there is also a dynamic response to interventions, resulting from discharge fluctuations and local variations in the river's geometry (e.g., Howard, 1982; Van der Klis, 2003; Chatanantavet and Lamb, 2014; Arkesteijn et al., 2019). Note the effect of the dynamic fluctuations is not shown in Fig. 1B. At local interventions, the largest dynamic response of the bed level occurs just downstream of the start and end of the intervention. These bed level changes are associated with a hydrograph boundary layer that results from an imbalance between the local sediment supply and local sediment transport capacity (Blom et al., 2017; Arkesteijn et al., 2019). This temporal imbalance leads to waves of bed level variation that migrate and diffuse in downstream direction (e.g., Wong and Parker, 2006; An et al., 2017a,b). Local interventions create such a temporal imbalance by withdrawing discharge from the main channel or creating gradients in the channel geometry. Note that the dynamic response (in terms of bed level change) can be an order of magnitude larger than the average response depending on the type of intervention (Van der Klis, 2003).

On a *large spatial scale*, we find bed level changes that are a system-wide response to the large-scale engineering measures of the past. In the river Waal (the main Rhine branch in the Netherlands), this response is governed by a decrease in the river bed slope that manifests itself in degradation in the upstream reaches (rkm 860–910) and aggradation in the ones downstream (rkm 910–950) with a maximal bed level change rate of about 2 cm/yr (Blom, 2016; Ylla Arbós et al., 2019). This is not true for any engineered delta, in which generally sediment deposits in the estuary, and it is also not true for pristine rivers, in which deltas tend to prograde (Chavarrías et al., 2018). In this paper, we focus on bed level changes that are dominated by the river discharge, i.e., the studied intervention is sufficiently away from the sea.

For river management, it is important to be aware of these three different scales. The observed local bed-level change can be partly attributed to the large-scale engineering measures from the past, partly to local interventions and partly to the presence of local structures such as groynes. Each scale causes different problems for management. The large-scale (>10 km) bed degradation can destabilize man-made structures (sluices and weirs) and limited access to harbors (e.g., Habersack et al., 2016; Hiemstra et al., 2020). Local interventions generally cause a bed-level increase on an intermediate scale (100 m–10 km), and this might increase dredging needs to support navigation. The small-scale bed-level changes (<100 m), such as bedforms, are much more local and variable, are therefore less important from a maintenance point of view. When undertaking new interventions, a good estimation of the

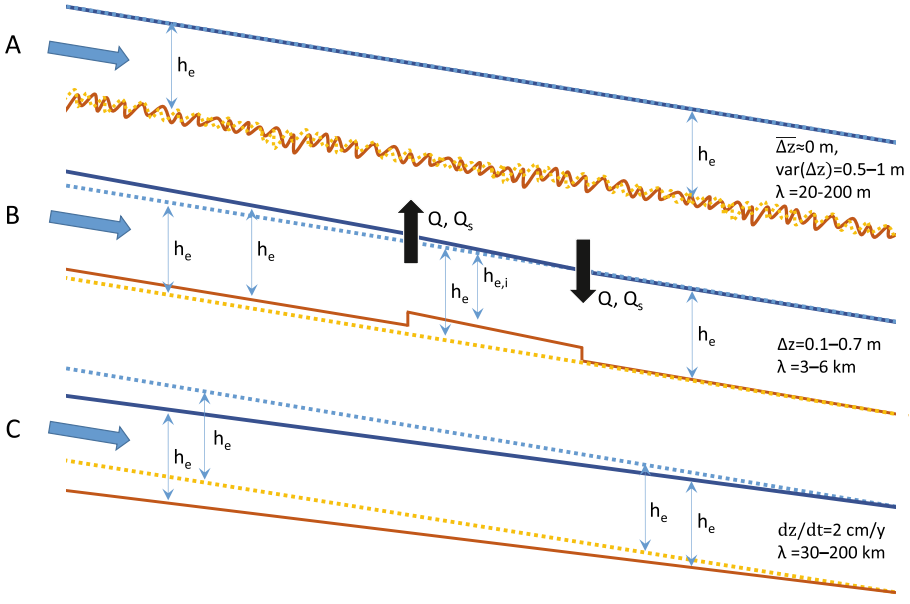

Fig. 1. (A) the bed level variation resulting from bedforms with an expected bed amplitude of 0.5–1 m with a wavelength (λ) of 20–100 m (Wilbers and Ten Brinke, 2003). The time-averaged change (Δz) is approximately zero. (B) The contribution of the intervention after a new equilibrium state is reached. A local intervention results typically in a change of 0.1–0.7 m (depending on the scale of the intervention). (C) The contribution of the large-scale adjustment (Δz = 2 cm/yr and λ = 30–200 km (Ylla Arbós et al., 2019)). Dashed lighter lines (bed level and water level) denote the situation before the intervention. Solid dark lines denote the situation after the intervention. Q and Q_s show the withdrawal and the insertion of the water and sediment discharge resulting from the intervention. The equilibrium depth is denoted by h_e (outside the influence of the intervention) and h_{ei} (at the intervention, and $h_{ei} < h_e$ due to the discharge withdrawal). The vertical scale is exaggerated.

resulting bed level change is crucial for heavily navigated rivers such as the river Waal (The Netherlands). Excess channel aggradation increases dredging costs or reduce the river's navigability, which has economic consequences (Havinga et al., 2009; Van Vuren et al., 2015). By disentangling the different spatial scales from the total channel response and isolating the intermediate scale, we can identify specifically the impact of interventions. To achieve this, we analyze high-resolution bi-weekly multi-beam measurements (2004–2020) of the navigation channel of the river Waal in the Netherlands. We focus on the effect of a side-channel construction on the local bed level and disentangle the three scales over which morphological changes take place using a wavelet transform. We compare the measured bed-level change on the intermediate scale with the results of a simple analytical model based on equilibrium theory (Appendix A). We show that the analytical model can be applied to assess the morphological changes resulting from interventions.

2. Method

We use multi-beam echo-sounder measurements to study the bed level changes in the main channel at a side-channel construction in the river Waal (Fig. 2). Changes in the bed level result from an imbalance between the sediment supply and the local sediment transport capacity. This imbalance is studied in one dimension along the river axis, meaning that we transform the multi-beam data (x, y, z) to a width-averaged bed level along the river axis (s, z) and ignore the cross-sectional redistribution of sediment. We apply a wavelet transform on the width-averaged longitudinal bed level to disentangle the spatial scales of bed level changes.

2.1. System description

The river Waal is a gravel/sandbed river with a yearly-averaged sediment load of approximately 200,000 m^3/yr (Frings et al., 2015, 2019). Fig. 3 shows the discharge in the river Rhine at Lobith (Fig. 2) between 2000 and 2019. The river Waal conveys about 2/3 of the river Rhine's discharge. To keep the river Waal navigable, continuous dredging activities occur. Since 1992, sediment extraction from the river is regulated. The largest part of the sediment that is dredged to maintain the water depth is dumped in deeper areas of the channel to maintain the sediment balance of the river (Sieben, 2009). Still, about 210,000 m^3 of

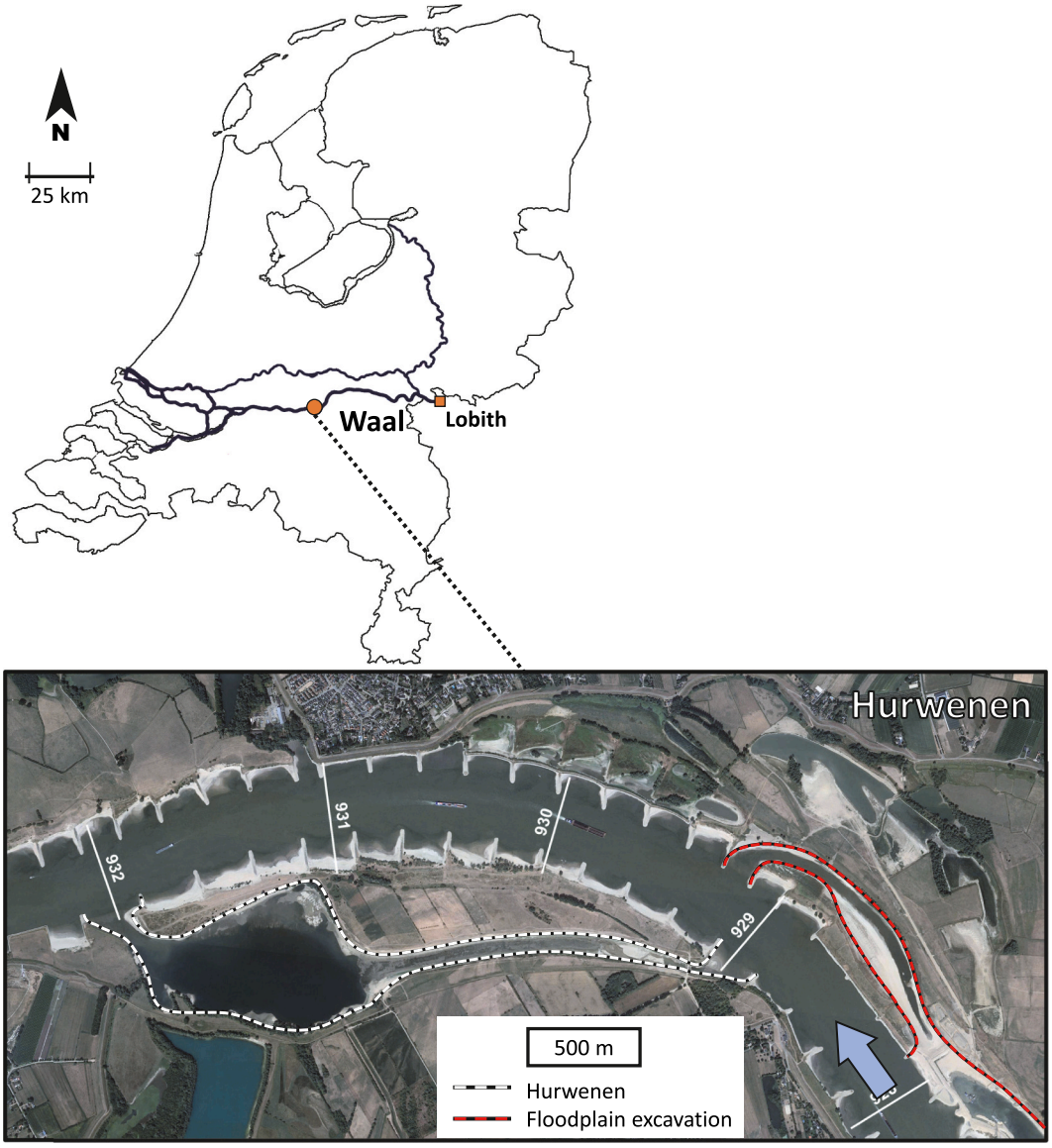

Fig. 2. The side channel constructed in the river Waal (Aerial image of 2018; Source: Google Earth). The aerial image also shows the location of the floodplain excavation (2017–2019).

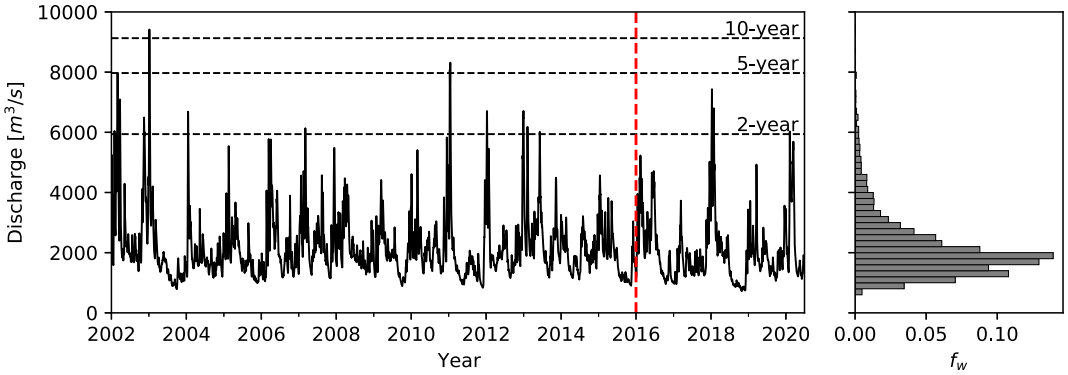

Fig. 3. Left: The daily discharge at Lobith in the river Rhine from 2002 to 2020 with the return periods of the peak discharges. The dashed vertical line denotes the moment of the side-channel construction. Right: The discrete probability density function of the discharge at Lobith in the river Rhine based on measurements between 2002 and 2020. (Data: https://waterinfo.rws.nl; return periods discharges (Hegnauer et al., 2014)).

sand was yearly extracted from the river Waal up to the summer of 2018.

The side channel near Hurwenen in the river Waal (river kilometer (rkm) 929–932; 51°49′4.17″ N; 5°18′0.05″ E) was constructed in 2015 and is located in an inner bend (Fig. 2). The side channel connects a sand-mining pit located in the floodplain with the main channel and the discharge is regulated by a weir that has a culvert. The maximum discharge withdrawal by the side channel is estimated to be 2.5% of the total discharge. Based on static equilibrium theory (Appendix A), it is expected that due to the intervention the bed level in the main channel increases with 0.10–0.13 m depending on whether the intervention also extracts sediment from the main channel.

Other interventions also affect the bed level in this region of the river. (1) Just upstream of the side channel, a non-erodible layer was constructed (1996) in the outer bend to reduce the aggradation in the inner bend and thereby, increase the width of the navigation channel. This has resulted in a large scour hole just downstream of the non-erodible layer that extends almost to the entrance of the side channel. (2) The height of the groynes in the river was reduced in 2015 over almost the full length of the river Waal and this causes large-scale aggradation in the main channel. (3) The floodplain opposite to the one with the side channel was excavated between 2017 and 2019 (Fig. 2). This excavation includes the construction of a floodplain channel that is only connected with the main channel at its downstream end. This intervention can also cause aggradation in the main channel over the same spatial scale as the side channel but the aggradation is expected to be smaller. By applying the wavelet transform, most bed level changes resulting from those other interventions are removed. Others have a relatively small effect on the bed level compared to the bed level change resulting from the side channel at Hurwenen.

2.2. Bed level measurements

The bed level of the navigation channel in the river Waal is measured biweekly (2004–2020) using multi-beam echo sounders. These bed level measurements give detailed information on the bed level's temporal and spatial variation within the navigation channel. The measurements are processed to rasters (2005–2011: 2.5 × 2.5 m; 2011–2020 1 × 1 m) using a 95% confidence filter to meet Dutch standards for hydrographic surveys (Rijkswaterstaat, 2009). There are at least 10 data points for at least 95% of the raster cells, but the point density is generally much larger (De Ruijsscher et al., 2020). We average the bed level over the width of the navigation channel by averaging the raster data over a strip of 5 m (longitudinal direction) times 150 m (transversal direction) Van Denderen et al. (2022). The navigation channel is about half the main channel's width and is generally located in the river's outer bends. Therefore, bed level changes derived from this data can be affected by the redistribution of sediment from the outer bend to the inner bend. This indicates that the analysis of the navigational channel data might lead to an overestimation of the temporal bed level changes compared to performing analysis over the full cross-section.

We study the changes in bed level relative to a reference bed level. Between 2014 and 2016 many interventions were constructed in the river Waal as part of Room for the River (Rijke et al., 2012; Van Vuren et al., 2015). Since these interventions can already affect the bed level during the construction phase, we define the reference bed level as the average bed level between January 2005 and January 2014 for each 5 × 150 m strip. We evaluate the bed level changes relative to the reference bed level and apply the wavelet transform to the spatio-temporal data set. We will show that with the wavelet transform, we can isolate changes in the bed level that can be contributed to local interventions.

2.3. Wavelet transform

A wavelet transform can be used to identify frequencies in a wave-like signal. The advantage of a wavelet transform above a Fourier transform is that it can analyze a non-stationary signal (in time or space), or, worded differently, a wavelet transform can identify wavelengths that vary in time or space. The wavelet transform has been widely applied to identify and characterize geophysical phenomena such as turbulence structures (e.g., Farge, 1992; Nicolleau and Vassilicos, 1999; Hardy et al., 2009; Yuan et al., 2009), river meanders (e.g., Gutierrez and Abad, 2014; Vermeulen et al., 2016), river bedforms (e.g., Gutierrez et al., 2013) and river bed topography (e.g., Keylock et al., 2014). The response of the riverbed due to the variations in the water and sediment discharge is different for each spatial scale, varying from small scale due to e.g. the rhythmic pattern of groynes, via an intermediate scale due to interventions in floodplains to a large scale due to large scale-engineering measures like channel narrowing and straightening. A wavelet transform is ideally suited to identify the bed level changes on those different spatial scales, where a Fourier-analysis would only reveal dominant frequencies under the assumption that they are equally present over the complete domain. In our case, the wave-like signal is given by the temporal-spatial variation of the bed-level profile relative to the time-averaged bed-level profile. The temporal and spatial changes in the bed level show whether scour (negative) or deposition (positive) occurred over time with respect to the reference bed level. First, we analyze a single spatial signal (the longitudinal bed-level profile derived from multi-beam echo-soundings) and then, we study the temporal development of that longitudinal bed-level profile.

The results of a wavelet transform depend on the chosen mother wavelet. Some mother wavelets such as the Mexican-hat can be used to distinguish abrupt changes in space in the signal (i.e. a good spatial resolution) but have a poor frequency resolution (Torrence and Compo, 1998; Addison, 2002). Comparing this to Fourier analysis, the poor

frequency resolution is to say the analysis reveals a broad peak in the power spectrum, causing a signal with a single wavelength to be transformed into a spectrum covering a range of wavelengths. In literature, this is called an 'energy leak', which we must consider when filtering for specific spatial scales of bed level changes. In the case of spatial and temporal riverbed data, we require both a good spatial resolution (such that we can relate bed level changes to local interventions) and a good frequency resolution (such that we can distinguish between the spatial scales of bed level changes). We choose the Morlet wavelet as the mother wavelet as it is an optimal balance between the spatial and frequency resolution (Torrence and Compo, 1998; Addison, 2002). The Morlet wavelet is a well-known and commonly applied mother wavelet but is not exactly analytic because it has a non-zero mean (Addison, 2002; Kirby and Swain, 2013). This error is negligible for $\omega_0 > 5$ and, therefore, the Morlet wavelet can still be used in practice (Farge, 1992; Addison, 2002; Kirby and Swain, 2013). The range of wavelengths that, due to the energy leak, is affected by single wavelength can for a Morlet wavelet be estimated using (Kirby and Swain, 2013):

$$\frac{\omega_0}{\lambda_{bandwidth}} = \frac{\omega_0}{\lambda} \pm \frac{\sqrt{-2lnq}}{\lambda} \tag{1}$$

where λ is the equivalent Fourier wavelength of the wavelet, ω_0 is the non-dimensional frequency of the Morlet wavelet chosen to be six (Torrence and Compo, 1998), q is the fraction of the signal that is left, and $\lambda_{bandwidth}$ is the minimal and maximal wavelength at which a signal with scale λ is still present with a fraction q. We assume that the signal is negligible if $q = e^{-2}$ (Torrence and Compo, 1998) resulting in $\lambda_{bandwidth} = \left[\frac{3}{4}, \frac{3}{2}\right]\lambda$.

The impact of local interventions is found by determining the range of wavelengths that are affected by the intervention. The lower limit for filtering is given by the bed level variations resulting from bedforms and groynes. Groynes are placed regularly every 200 m and thereby force a bed level variation with a wavelength of 200 m. The wavelength of bedforms is in the river Waal smaller, even during peak flow conditions (Wilbers, 2002). Taking into account the bandwidth of the frequency resolution (Eq. (1)) this results in a lower limit of $\lambda = \frac{3}{2} \cdot 200 = 300m$.

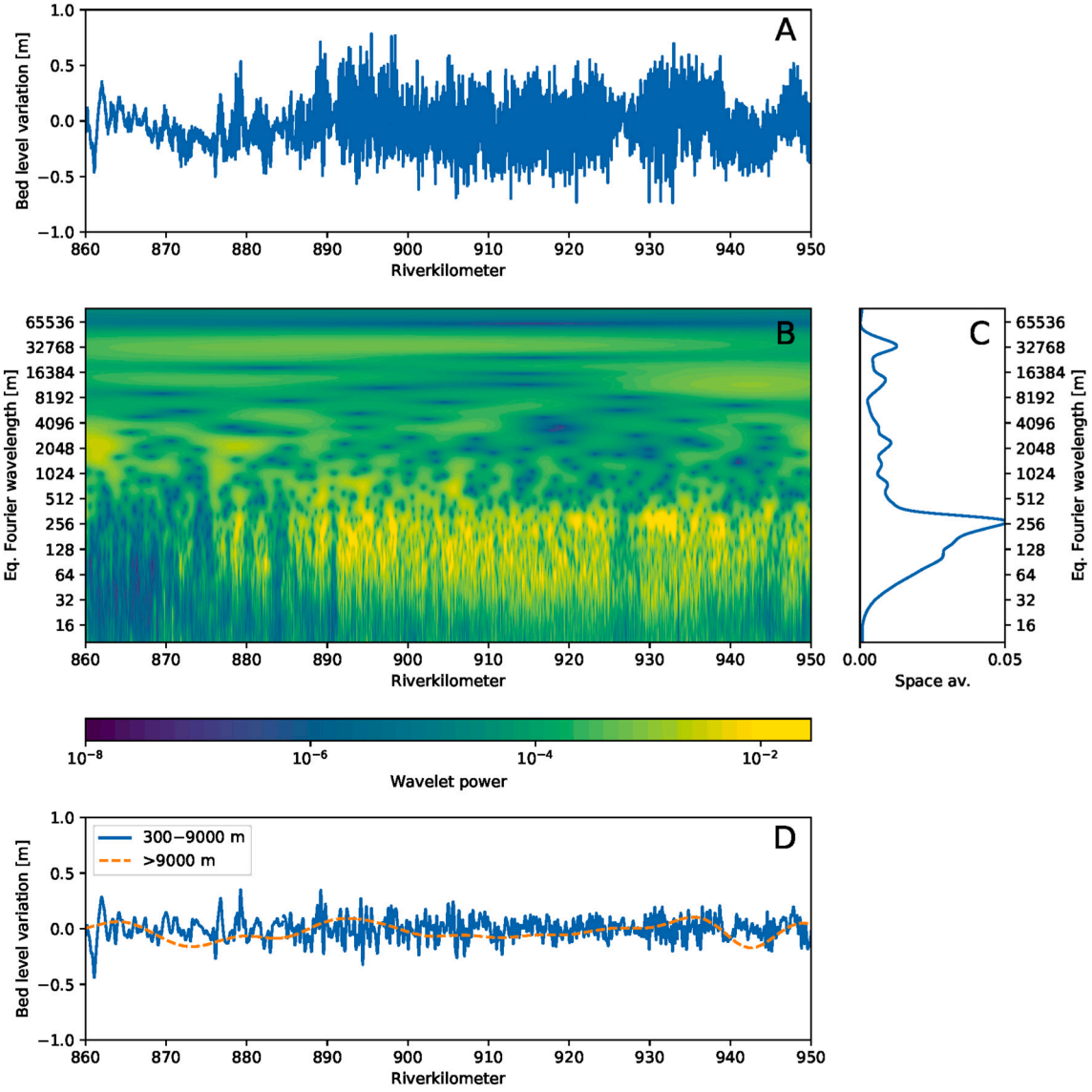

Fig. 4. (A) The bed level variation for the river Waal from January 2014 relative to the time-averaged bed level. (B) The wavelet power spectrum as a function of the river kilometer and the equivalent Fourier wavelength. (C) The global wavelet power spectrum for January 2014. (D) The filtered signal for 300–9000 m and >9000 m.

The upper level for filtering is determined by the expected morphological response of the intervention, which is 3 km long. Following equilibrium theory (Jansen et al., 1979; Van der Klis, 2003; De Vriend, 2015), we expect aggradation in the main channel over the full length of the intervention corresponding to a Fourier wavelength of 6.0 km. This results in an upper filtering limit of $\lambda = \frac{3}{2} \cdot 6000 = 9\,km$ (Eq. (1)).

3. Results

3.1. Wavelengths in the river Waal

We apply the wavelet analysis on the bed level measurements in the navigation channel of the river Waal relative to the time-averaged bed level. Fig. 4A shows the bed level variation around the time-averaged bed level between rkm 860–950 for January 2014. The wavelet power spectrum of the signal (4B) indicates the intensity of the Morlet-wavelet for a certain location and an equivalent Fourier wavelength (λ). Fig. 4B shows a large variation of the wavelet power over the domain and thereby the benefit of a wavelet transform with respect to a Fourier-transform. A Fourier transform does not take into account the variation of the frequencies over the spatial domain. In Fig. 4C, we average the power spectrum over the river stretch, i.e. the global wavelet power spectrum. Although we then lose the specific spatial information of the distribution of the wavelet power spectrum, it enables us to localize the peaks in the equivalent Fourier wavelengths distribution.

The wavelet transform shows that there is little energy for $\lambda < 256$ m

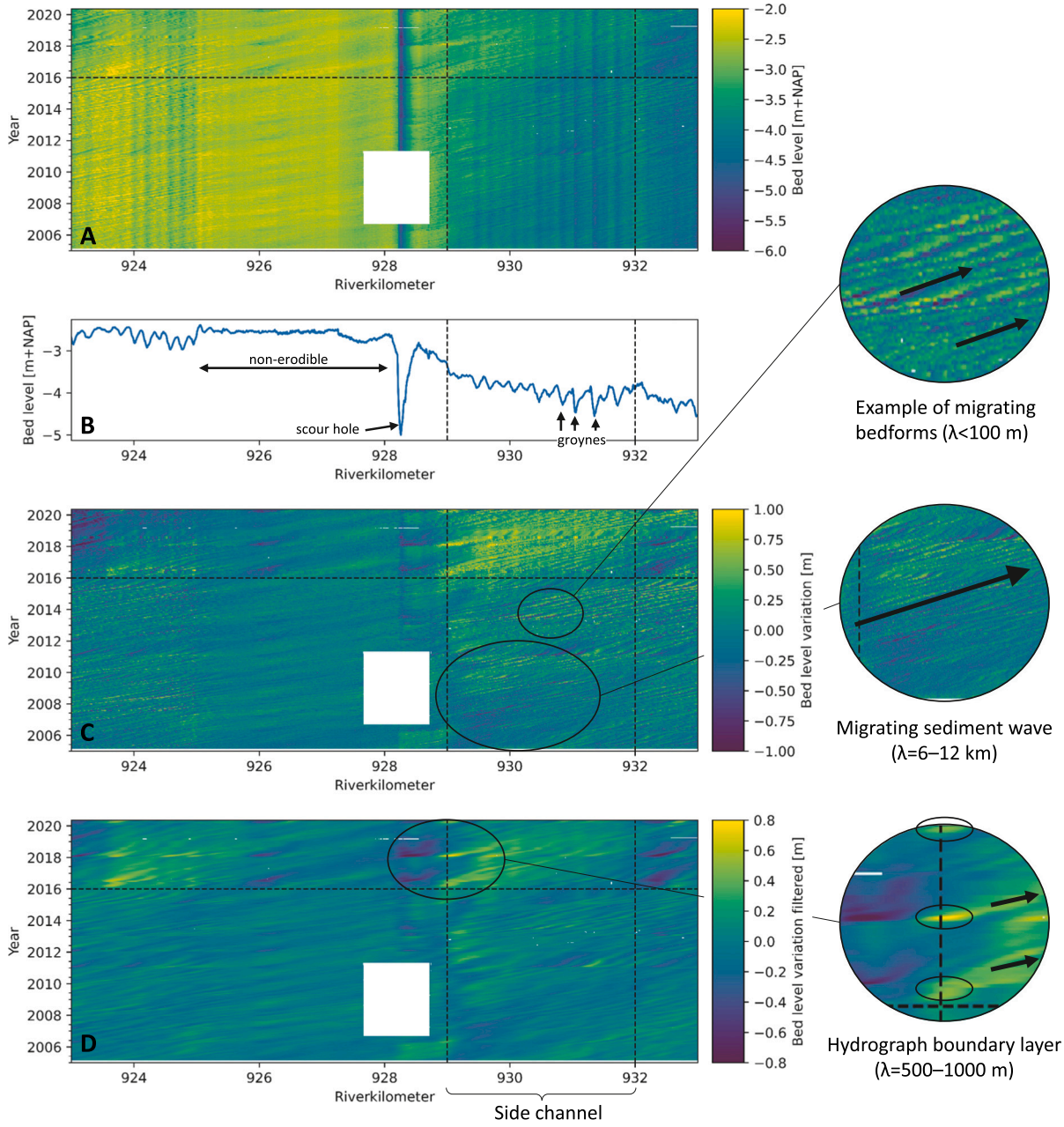

Fig. 5. The bed level in space and time near the side channel of Hurwenen. The white boxes and lines are areas with no data and the dashed lines denote the bifurcation and confluence, and the moment of construction of the side channel. (A) The width-averaged bed level in the navigation channel at Hurwenen. (B) The width and time-averaged bed level before intervention (2005–2014). (C) The bed level variation, i.e. the time-averaged bed level (B) is subtracted from the bed level (A). This is the equivalent of Fig. 4A for all dates between 2004 and 2020. (D) The filtered bed level variation based on the wavelet transform applied to the data set represented in (C). This is the equivalent of Fig. 4D (filtering between 300 m and 9000 m) for all dates between 2004 and 2020.

at rkm 860–870, but considerably higher energy for $\lambda < 256$ at rkm 880–950. The bed material at rkm 860–870 is much coarser (Ylla Arbós et al., 2021) and thereby less mobile. This results in smaller bed level variations near groynes ($\lambda \approx 200$ m) and in smaller bedforms ($\lambda \leq 100$ m) that migrate more slowly. The reduced morphological activity at rkm 860–870 causes smaller and fewer deviations from the time-averaged bed level and hence low energy in the wavelet power spectrum.

Between $300 < \lambda < 9000$ m, there are several peaks in the power spectrum, but there is not a clear wavelength that is present over the full reach. For example, at rkm 860–865 and rkm 875–880 there are energy spots for $1024 < \lambda < 2048$ m. At rkm 860–865 this is a result of a migrating bar in the channel. At rkm 875–880 the energy spot results from a point bar in the inner bend that grows as a function of discharge fluctuations. Fig. 4D shows the bed level variation that corresponds to the intermediate spatial scale. Each peak in the power spectrum in Fig. 4D is related to sedimentation or erosion on a certain spatial scale that can be a result of the river planform, recent hydrodynamic conditions or migrating sandbars.

For large wavelengths ($\lambda > 9000$ m), we find peaks in the energy spectrum at 16 km and 32 km that correspond to bed level changes on a large spatial scale. This is most probably due to the large-scale channelization interventions, and to large-scale variations in the planform of the river. Filtering the bed level variations (Fig. 4A) for $\lambda > 9000$ m results in the orange dashed line in Fig. 4D that can be interpreted as the large scale degrading response of the river. The degrading character is reflected by the fact that the orange dashed line includes mainly negative values. The figure shows that the large-scale bed level variation is in the same order of magnitude as the one on an intermediate spatial scale.

3.2. Morphological effects of the side channel Hurwenen

In this section, we study the morphological changes resulting from the construction of the side channel near Hurwenen. Similar to Fig. 4D, each bed level profile is filtered to extract the bed level variation on an intermediate spatial scale ($300 < \lambda < 9000$ m).

3.2.1. Spatial and temporal bed-level variation

We focus on a 10 km long stretch of the river Waal (rkm 923–933) where the side channel was constructed in 2016 (Section 2.1). Fig. 5A shows the unfiltered bed level development in space and time. Each horizontal line in the figure represents the width-averaged bed level (Section 2.2) at a moment in time. The figure contains nearly 400 bi-weekly measurements. Fig. 5A shows both steady and migrating features. The steady features result from the geometry of the river or structures in the channel. These steady features are also visible in the reference bed level (Fig. 5B), which is the bed level averaged over January 2005–January 2014. For example, rkm 925 to 928 of the navigation is non-alluvial and consists of a non-erodible fixed layer of coarse stones. The downstream response to this fixed layer is a large scour hole at rkm 928. In addition, a pattern of steady bed level features with a much smaller wavelength is present almost over the full remaining stretch from rkm 923–925 and 928–933 (Fig. 5A and B). This is the local response to the groynes. Fig. 5C shows the temporal bed level variation around the time-averaged longitudinal bed level (i.e. the temporal compilation of Fig. 4A). In Fig. 5C, the migration of small bedforms and the migration of larger sand bars is clearly visible. In addition, larger sediment waves seem to migrate through the system. For example, just upstream of rkm 930, the bed is slightly lower up to 2008 compared to the time-averaged bed level. This lower bed migrates through the system as a degradation wave (Fig. 5C). From 2008 onwards, the bed level just upstream of rkm 930 is slightly higher compared to the time-averaged one and this elevation migrates downstream as an aggradation wave. Such migrating sediment waves are likely a result of upstream disturbances resulting from structures, interventions or discharge fluctuations that migrate through the river.

We apply the wavelet filtering to the dataset depicted in Fig. 5C to remove the small (<300 m) and large (>9000 m) scale bed-level variations (Fig. 5D). Dark colors indicate bed levels below average, light colors indicate bed values above average. The filtered bed-level variation shows that before December 2015 the bed level variation is, generally speaking, much smaller than after 2015. A peak discharge in 2011 (before the construction of the intervention) causes larger deviations from the time-averaged bed level. This is, among others, a result of local variations in the floodplain geometry and corresponds to the dynamic response of the river to discharge fluctuations (Arkesteijn et al., 2019).

After the construction of the side channel, peak flow conditions in 2016, 2018 and 2020 cause deposition up to 0.79 cm at the bifurcation with the side channel (yellow colors in Fig. 5D). The deposited sediment migrates downstream with a celerity of about 1 km/year, diffuses and develops into an average bed level increase. The opposite occurs just downstream of the side channel where scour occurs during each peak flow event (2016, 2018 and 2020). This deposition in the main channel results from an imbalance between the sediment supply, which did not change, and the sediment transport capacity, which changed due to the discharge withdrawal of the side channel, and resembles a hydrograph boundary layer. The scour just downstream of the side channel results from a reduced sediment supply, due to the deposition just upstream, and the sediment transport capacity that did not change.

Another component that enhances the bed level variation at the upstream end of the intervention is the scour hole downstream of the non-erodible layer. The depth of this scour hole increases during every peak flow and part of this feature migrates downstream after the peak flow. This migration might mitigate the bed level increase that results from the intervention.

3.2.2. Change in the longitudinal profile

Fig. 6 shows the time average of the filtered spatial bed level variation (Fig. 5D) together with the 5 and 95% percentiles along the river axis before (averaged from January 2005 to January 2014) and after the intervention's construction (averaged over January 2016 to December 2019). Before the construction of the intervention, the average bed level variation is zero because it equals the reference bed level. The bed level varies approximately −20 cm and 20 cm around the average due to discharge fluctuations and the migration of the degradation and aggradation waves (Fig. 5D). The average bed level after 2016 shows that aggradation occurred over the length of the side channel (Fig. 6A). The largest bed level variation occurs at the upstream end of the intervention and this variation reduces in the downstream direction. This corresponds with the local deposition during peak flow events that migrate downstream during lower flow conditions (Fig. 5D). In 2019, the peak flows were relatively small compared to the one in 2018. Therefore, the average bed-level change in 2019 (January–December) is smaller in the upstream part than the average bed-level change in 2018 (Fig. 6B). The bed level in the upstream part of the intervention is most affected by discharge variations because here the largest gradient in transport capacity occurs. The downstream part has not changed much between 2018 and 2019. The variation in the average bed level is partly related to the transient phase towards the new quasi-equilibrium but is likely also related to the hydrodynamic boundary layer that results from discharge fluctuations. From Fig. 6A, it is also clear that the dynamic response of the bed level change (visualized by the 95% percentile) can be 6 times higher than the static component (the orange dashed line). The bed level variation shows that the scour hole deepens in years with peak flow conditions (2018) and becomes more shallow in years without peak flows (2019). Such trends are visible along the river where geometry variations occur.

3.2.3. Average bed level change on intermediate and large scale

The advantages of using the wavelet transform and the associated filtering become clear by comparing the bed-level change averaged over the length of the intervention (3 km) with the unfiltered data. In Fig. 7A,

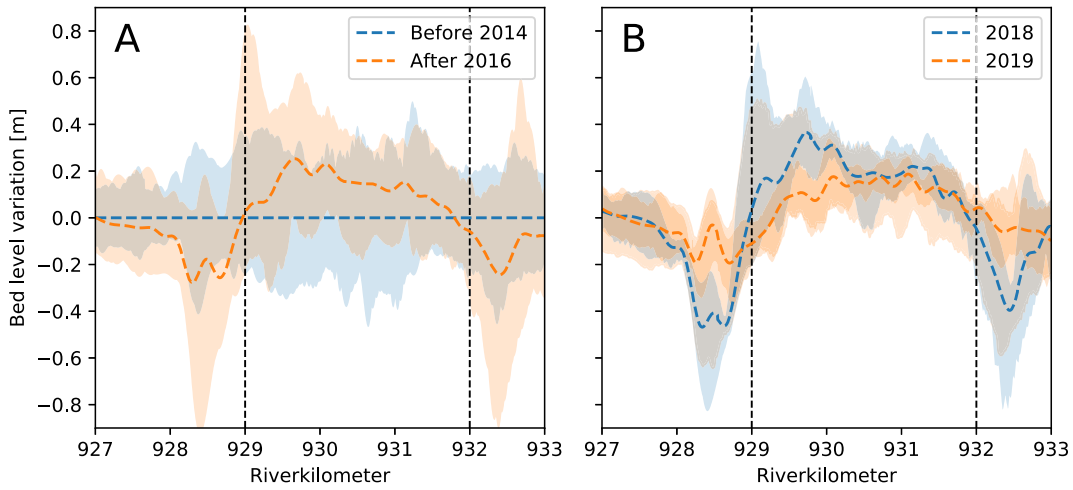

Fig. 6. (A) The average bed level with the 5% and 95% percentile before and after the construction of the intervention. (B) The average bed level with the 5% and 95% percentile of 2018 with a peak flow event and of 2019 without a peak flow event. The dotted lines show the location of the bifurcation and the confluence of the intervention. Note that the dashed lines are the equivalent of Fig. 5D for the years 2018 and 2019.

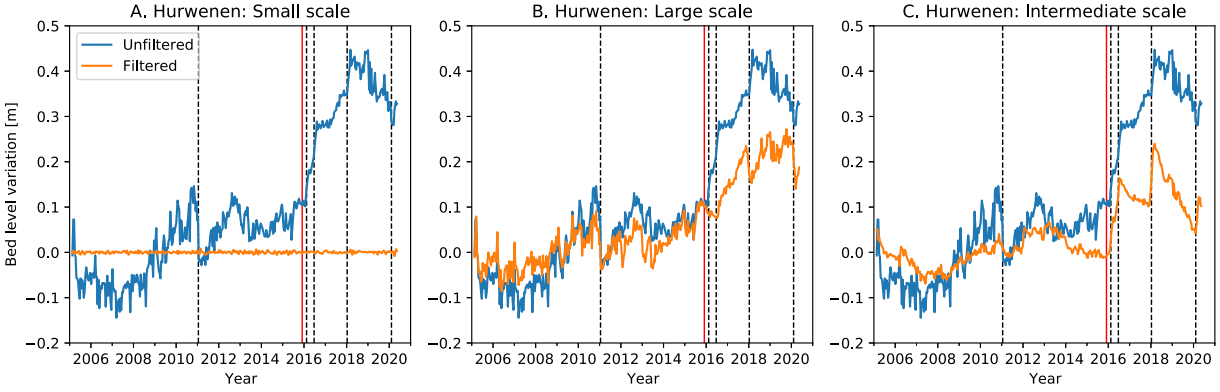

Fig. 7. The unfiltered bed level variation in time and the filtered bed level variation for the three spatial scales averaged over the length of the side channel. The vertical red line shows when the side channel was constructed. The dashed vertical lines denote the occurrence of peak flow discharges to which we refer to in the text (Fig. 3). (For interpretation of the references to color in this figure legend, the reader is referred to the web version of this article.)

we filter over all wavelengths up to 300 m. This reflects the changes of small-scale elements like the groynes or bedforms. The filtered signal is zero because the small-scale bed-level variations (<300 m) do not contribute to the bed level averaged over 3 km.

Fig. 7B shows the result of filtering for all wavelengths larger than 9 km. This reflects the contribution to the bed level changes originating from large-scale variations in the river geometry and possibly long-term temporal effects due to narrowing and shortening of the river in the past. The filtered large-scale bed level change shows a clear overall aggrading trend (Fig. 7B). However, during peak discharges in 2011, 2016, 2018 and 2020, degradation seems to occur. This is likely related to a redistribution of sediment over the cross-section resulting in a net transverse sediment transport out of the navigation channel during floods (recall that the bed level data only covers the navigational channel).

The intermediate scale bed level variation (300–9000 m) shows a variation around zero until 2016, the time of construction of the intervention (Fig. 7C). This variation corresponds with the spatially migrating degradation and aggradation waves (Fig. 5D) that originate from variations in discharge. In 2016, the first discharge peak occurred since the construction of the side channel. The peak discharges in 2016, 2018 and 2020 cause aggradation in the main channel (where the long-wavelength filtering showed degradation). Apparently, the average bed level quickly starts to decrease after the passing of the flood wave due to the migration and diffusion of the local sediment peaks (Fig. 5D). This decrease of the bed level is likely enhanced by the downstream migration of the scour hole that results from the non-erodible layer which is enlarged after peak flow conditions. The increase and decrease of the average bed level repeat themself during each peak flow and results in a large variation of the average bed level in time. The space and time-averaged bed level change from 2016 to 2020 is 12.5 cm and this is similar to the estimation based on analytical relations (Appendix A). The results depicted in Fig. 7A–C show the added value of the wavelet analysis. If one only considers the unfiltered signal, one is inclined to estimate the consequences of the intervention to be around 40 cm aggradation. However, the wavelet analysis shows that almost half of this effect comes from long spatial and temporal term responses and the effect due to the intervention is more in the order of 12.5 cm. Regarding operations and maintenance, the river manager should take into account the latter rather than the first, when assessing the morphological consequences of the measure.

4. Discussion

4.1. Wavelet filtering

The wavelet transform allows for the filtering of bed level changes that occur at various spatial scales. By disentangling the large, intermediate and small-scale bed level variations, we can isolate their impact

on the local bed level change. The contribution of each spatial scale varies along the river and in time. Fig. 7 shows that, with the wavelet filter on the intermediate scale, we remove the long-term and large-scale trend. This trend varies in time and space and causes a bed level change in the same order of magnitude as local interventions. Using the unfiltered result would lead to an overestimation of the impact of local interventions.

The limits of the wavelet filtering depend on the type and scale of the intervention. The lower limit is related to features such as dune-like bedforms and groynes and the intervention's length determines the upper limit. Here, we can distinguish the impact of the intervention from the large-scale bed-level change since the wavelengths are sufficiently apart. It becomes more difficult if the aggradation resulting from the intervention occurs on the same spatial scale as the large-scale bed degradation. Also, the chosen mother wavelet affects the final result. For example, using a Mexican hat wavelet, which has a lower frequency resolution, it would be more difficult to distinguish between wavelengths and, thereby, to filter based on the wavelength. The Morlet wavelet is an optimal balance between the frequency and spatial resolution and is therefore used here.

4.2. Prediction methods for aggradation

We evaluated the bed level change in the main channel as a result of side-channel construction in the river Waal. The side channel withdraws discharge from the main channel reducing the sediment transport capacity and thereby increasing the bed level. The bed level is expected to increase over the full length of the intervention based on equilibrium theory (Jansen et al., 1979; De Vriend, 2015). Interventions also cause a dynamic response of the riverbed and this dynamic response is much larger (up to a factor 6) (Fig. 6A). The dynamic response quickly disappears with changing discharge. An intervention that withdraws discharge from the main channel will, generally, cause large deposition at the upstream side of the intervention and large scour just downstream. This deposition and scour continuously develop, migrate and diffuse due to discharge variations in the river. This dynamic component results from an imbalance between the sediment supply and the sediment transport capacity as a function of the discharge, i.e. the intervention creates a hydrograph boundary layer (e.g., Wong and Parker, 2006). The resulting bed level changes are relatively large during peak flow conditions, but they quickly disappear with decreasing discharge.

The dynamic component of the river's equilibrium bed level is not just affected by recently constructed interventions, but also includes bed level changes resulting from previously constructed interventions or the floodplain geometry. For example, the fixed layer at rkm 925–928, the construction of a floodplain channel at rkm 928–929, the narrowing of the floodplain in the river Waal at rkm 930.5. These cause morphological changes on the same wavelengths as the morphological changes caused by the side channel Hurwenen. The fixed layer creates a scour hole just downstream rkm 928.5 that deepens during peak flow conditions (Fig. 5). Both the floodplain channel and the narrowing of the floodplain only cause bed level changes during peak flow conditions. These will increase the dynamic response of the river to flow fluctuations but have a limited effect on the time-averaged bed level.

5. Conclusion

The wavelet transform can be used to disentangle various contributions to the local bed level changes based on their spatial scale. We apply the method specifically to estimate the bed level changes that occur after the construction of a side channel and compare these changes with theoretical estimates. Locally, the bed level is affected by large-scale changes due to engineering works of the past and small-scale changes that result from dune-like bedforms. River interventions, generally, affect the bed level on an intermediate spatial scale. With the wavelet filtering, we can separate the small, intermediate and large-scale bed level changes even when the magnitude of bed level changes are in the same order.

Using the wavelet analysis, we can isolate the bed level change caused solely by the construction of a side channel and find that several years after construction, the space and time-averaged bed level increase in the main channel corresponds with the theoretical estimate. In addition, the side channel also causes dynamic bed level fluctuations around the average bed level change. The magnitude of these fluctuations depends on discharge fluctuations and can be a factor 6 larger than the average bed level change. They quickly disappear with changing discharge. With wavelet filtering, we can disentangle the spatial scales that vary in time and space. This is beneficial for studying local bed level changes in rivers that have not yet reached their equilibrium state.

Declaration of competing interest

The authors declare that they have no known competing financial interests or personal relationships that could have appeared to influence the work reported in this paper.

Acknowledgments

This research is supported by the Ministry of Infrastructure and Water Management-Rijkswaterstaat and by the Netherlands Organisation for Scientific Research (NWO), which is partly funded by the Ministry of Economic Affairs, under grant number P12-P14 (RiverCare Perspective Programme) project number 13516. This research has benefited from cooperation within the network of the Netherlands Centre for River studies. We thank Susanne Quartel for her help and comments on the setup of this study.

Data availability

Datasets for this research are freely available. The raw multibeam data can be requested via Servicedesk Data Rijkswaterstaat (servicedesk-data@rws.nl). The bed level profiles can be found at https://doi.org/10.4121/19447043, hosted at 4TU.Centre for Research Data Van Denderen et al. (2022). The wavelet toolbox is provided by Torrence and Compo (1998).

Appendix A. Analytical model for the aggradation

We estimate the bed level changes in the main channel due to the construction of an intervention using analytical relations that describe the static equilibrium geometry of a river (e.g., De Vries, 1974; Jansen et al., 1979; Blom et al., 2017). We compute the static equilibrium before and after the construction of the intervention. We assume that (1) the intervention is constructed in the reach of the river that is governed by normal flow (i.e. we

ignore backwater effects), (2) the river has reached its static equilibrium geometry, (3) the static equilibrium geometry does not change except for the construction of the intervention, (4) after the construction of the intervention, a sufficient amount of time has passed such that a new static equilibrium state is reached, and (5) normal flow occurs everywhere in the river even after the construction of the intervention independent of the water discharge. In addition, we do not take into account the effects of floodplain flow or mixed-sediment processes.

A characteristic discharge needs to be defined to estimate bed level changes. Here, we use the slope-equivalent water discharge or channel-forming discharge that, given a yearly mean sediment supply, is the discharge at which the bed slope of the river is the same as the one that results from a long-term hydrograph (Following: De Vries, 1974, 1993; Jansen et al., 1979; Doyle et al., 2007; Blom et al., 2017). The channel-forming discharge ($Q_{w,dom}$) using Engelund and Hansen (1967) is given by:

$$Q_{w,dom} = \left[\int_0^\infty Q_w^{5/3} f_w(Q_w) dQ_w \right]^{3/5} \tag{A.1}$$

in which Q_w is the water discharge, $f_w(Q_w)$ is the probability density function of the discharge for a river. We apply Engelund and Hansen (1967) which computes both the bed-material and the suspended bed-material load. The same theory can be applied to other rivers using different sediment transport relations and taking into account mixed sediment processes following Blom et al. (2017). We assume that the channel-forming discharge is representative of normal flow depth in the river:

$$h_0 = \frac{Q_{w,dom}}{W} \left(\frac{W G_{EH}}{D} \frac{1}{\overline{Q}_s} \right)^{1/5} \tag{A.2}$$

in which h_0 is the water depth before the intervention, $Q_{w,dom}$ is the channel-forming discharge, W is the channel width, $G_{EH} = \frac{0.05 c_f^{3/2}}{\Delta g}$ is a parameter in the sediment transport relation of Engelund and Hansen (1967), D is the grain size, and $\overline{Q}_s$ is the average sediment transport. The construction of an intervention changes the channel-forming discharge in the main channel.

$$Q_{w,dom,i} = \left[\int_0^\infty \left(Q_w - \alpha(Q_w) Q_w \right)^{5/3} f_w \left(Q_w \right) dQ_w \right]^{3/5} \tag{A.3}$$

in which $\alpha(Q_w)$ is the fraction of the discharge that is withdrawn from the main channel as a function of the water discharge of the river. In addition, the sediment supplied to the side channel can reduce the sediment supply in the main channel. We assume here that the maximum sediment withdrawal occurs if the sediment partitioning at the bifurcation is proportional to the water discharge partitioning (Van Denderen et al., 2019a). This is a reasonable estimate for suspended bed-material load supplied side channels that commonly occur in the Rhine branches (Van Denderen et al., 2019b). The normal flow depth after the intervention then becomes:

$$h_i = \frac{Q_{w,dom,i}}{W} \left(\frac{W G_{EH}}{D} \frac{1}{\frac{Q_{w,dom,i}}{Q_{w,dom}} \overline{Q}_s} \right)^{1/5} \tag{A.4}$$

in which h_i is the normal flow depth in the main channel parallel to the side channel for $Q_{w,dom,i}$. The bed level increase in the main channel is given by:

$$\Delta z = h_0 - h_i \tag{A.5}$$

If we assume α to be constant, this results in:

$$\Delta z_{(\Delta Q_s)} = h_0 - h_0 (1 - \alpha)^{4/5} \tag{A.6}$$

This relation can be further simplified if we ignore the sediment withdrawal from the main channel due to the intervention:

$$\Delta z = \alpha h_0 \tag{A.7}$$

Most types of local river interventions can be simplified to a change in discharge conveyance in the main channel. We apply this to the side channel in the river Waal. These are derived from hydrodynamic computations that were made during the design of the intervention (Driessen and de Jong, 2011). We ignore the morphodynamic development of the interventions themselves, which, especially in the case of side channels, might be significant (e.g. Van Denderen et al., 2019b). The probability density function of the river Waal is shown in Fig. A.8. The maximum discharge withdrawal of the side channel at Hurwenen occurs at quite frequent discharges. Given the withdrawal of the side channel as a function of the discharge, the average aggradation in the main channel is estimated using Eqs. (A.1)–(A.4) with the parameters of Table A.1.

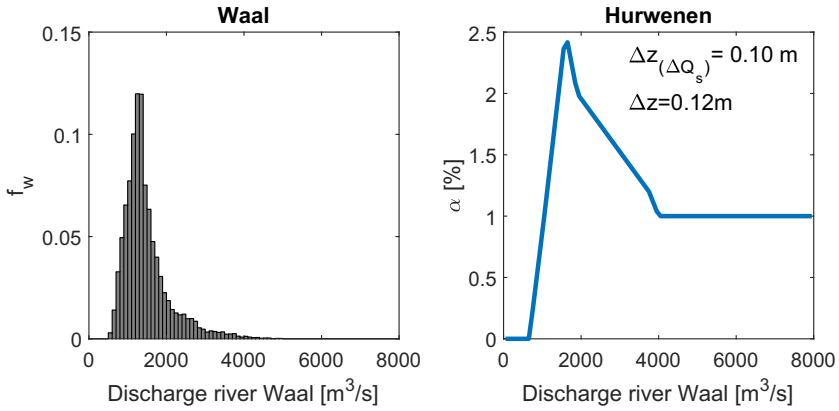

Fig. A.8. The probability density functions of the discharge in the river Waal and the discharge withdrawal from the main channel due to the construction of the side channel with the corresponding estimates for the average bed level increase in case of sediment withdrawal (Δz) and without sediment withdrawal (Δz_{nosed}). (Source discharge data: http://waterinfo.rws.nl).

Table A.1
The parameters used to estimate the average bed level change that is caused by the interventions as given in Fig. A.8.

Parameter	Value (Waal)	Reference
W	280 m	Becker et al. (2014)
D	1 mm	Ten Brinke (1997)
c_f	0.0058	Becker (2015)
$\overline{Q}_s$	200,000 m^3/yr	Frings et al. (2019)

References

Addison, P.S., 2002. The Illustrated Wavelet Transform Handbook: Introductory Theory and Applications in Science, Engineering, Medicine and Finance. Institute of Physics Publishing, Bristol, UK.

An, C., Cui, Y., Fu, X., Parker, G., 2017a. Gravel-bed river evolution in earthquake-prone regions subject to cycled hydrographs and repeated sediment pulses. Earth Surf. Process. Landf. 42, 2426–2438. https://doi.org/10.1002/esp.4195.

An, C., Fu, X., Wang, G., Parker, G., 2017b. Effect of grain sorting on gravel bed river evolution subject to cycled hydrographs: bed load sheets and breakdown of the hydrograph boundary layer. J. Geophys. Res. Earth Surf. 122, 1513–1533. https://doi.org/10.1002/2016jf003994.

Arkesteijn, L., Blom, A., Czapiga, M.J., Chavarrías, V., Labeur, R.J., 2019. The quasi-equilibrium longitudinal profile in backwater reaches of the engineered alluvial river: a space-marching method. J. Geophys. Res. Earth Surf. 124 https://doi.org/10.1029/2019JF005195.

Becker, A., 2015. Rijn-modellen 5de generatie Modelopzet, kalibratie en verificatie WAQUA. Technical Report. Deltares, Delft, The Netherlands.

Becker, A., Scholten, M., Kerhoven, D., Spruyt, A., 2014. Das behördliche Modellinstrumentarium der Niederlande. In: Dresdner Wasserbauliche Mitteilungen, 50, pp. 539–548.

Blom, A., 2016. Bed degradation in the Rhine River. URL. https://flowsplatform.nl/#/bed-degradation-in-the-rhine-river-1479821439344__47__.

Blom, A., Arkesteijn, L., Chavarrías, V., Viparelli, E., 2017. The equilibrium alluvial river under variable flow and its channel-forming discharge. J. Geophys. Res. Earth Surf. 122, 1924–1948. https://doi.org/10.1002/2017JF004213.

Buffington, J.M., 2012. Changes in channel morphology over human time scales. In: Church, M., Biron, P.M., Roy, A.G. (Eds.), Gravel-Bed Rivers: Processes, Tools, Environments. Wiley, Chichester, UK, pp. 435–463.

Chatanantavet, P., Lamb, M.P., 2014. Sediment transport and topographic evolution of a coupled river and river plume system: an experimental and numerical study. J. Geophys. Res. Earth Surf. 119, 1263–1282. https://doi.org/10.1002/2013jf002810.

Chavarrías, V., Blom, A., Orrú, C., Martín-Vide, J.P., Viparelli, E., 2018. A sand-gravel gilbertdelta subject to base level change. J. Geophys. Res. Earth Surf. 123, 1160–1179. https://doi.org/10.1029/2017JF004428.

Church, M., Ferguson, R.I., 2015. Morphodynamics: rivers beyond steady state. Water Resour. Res. 51, 1883–1897. https://doi.org/10.1002/2014wr016862.

De Ruijsscher, T.V., Hoitink, A.J.F., Naqshband, S., Paarlberg, A.J., 2019. Bed morphodynamics at the intake of a side channel controlled by sill geometry. Adv. Water Resour. 134 https://doi.org/10.1016/j.advwatres.2019.103452.

De Ruijsscher, T.V., Naqshband, S., Hoitink, A.J.F., 2020. Effect of non-migrating bars on dune dynamics in a lowland river. Earth Surf. Process. Landf. 45, 1361–1375. https://doi.org/10.1002/esp.4807.

De Vriend, H.J., 2015. The long-term response of rivers to engineering works and climate change. Proc. Inst. Civ. Eng. 168, 139–144. https://doi.org/10.1680/cien.14.00068.

De Vries, M., 1974. Sediment transport. In: Lecture Notes F10. Technical Report. Delft University of Technology, Delft, The Netherlands.

De Vries, M., 1993. Use of models for river problems. In: Technical Report. UNECO, Paris, France.

Doyle, M.W., Shields, D., Boyd, K.F., Skidmore, P.B., Dominick, D., 2007. Channel-forming discharge selection in river restoration design. J. Hydraul. Eng. 113, 831–837. https://doi.org/10.1061/(ASCE)0733-9429(2007)133:7(831).

Driessen, T., de Jong, W., 2011. Hurwenen - Maakbaarheid en vergunbaarheid: Hydraulica en Morfologie projectontwerp. Technical Report. Haskoning Nederland B.V, Nijmegen, The Netherlands.

Engelund, F., Hansen, E., 1967. A monograph on sediment transport in alluvial streams. In: Technical Report. Tekniskforlag, Copenhagen, Denmark.

Farge, M., 1992. Wavelet transforms and their application to turbulence. Annu. Rev. Fluid Mech. 24, 395–458. https://doi.org/10.1146/annurev.fl.24.010192.002143.

Formann, E., Habersack, H.M., Schober, S., 2007. Morphodynamic river processes and techniques for assessment of channel evolution in Alpine gravel bed rivers. Geomorphology 901, 340–355. https://doi.org/10.1016/j.geomorph.2006.10.029.

Frings, R.M., Banhold, K., Evers, I., 2015. Sedimentbilanz des Oberen Rheindeltas. Technical Report. Lehrstuhl und Institut für Wasserbau und Wasserwirtschaft, RWTH Aachen University, Aachen, Germany.

Frings, R.M., Hillebrand, G., Gehres, N., Banhold, K., Schriever, S., Hoffmann, T., 2019. From source to mouth: basin-scale morphodynamics of the Rhine River. Earth Sci. Rev. 196, 102830 https://doi.org/10.1016/j.earscirev.2019.04.002.

Gilbert, G.K., 1877. Report on the Geology of the Henry Mountains. Technical Report. URL. U.S. Government Printing Office, Washington, D. C. https://doi.org/10.3133/70039916.

Gregory, K.J., 2006. The human role in changing river channels. Geomorphology 79, 172–191. https://doi.org/10.1016/j.geomorph.2006.06.018.

Gutierrez, R.R., Abad, J.D., 2014. On the analysis of the medium term planform dynamics of meandering rivers. Water Resour. Res. 50, 3714–3733. https://doi.org/10.1002/2012WR013358.

Gutierrez, R.R., Abad, J.D., Parsons, D., Best, J., 2013. Discrimination of bedform scales using robust spline filters and wavelet transforms: methods and application to synthetic signals and the Rio Parana, Argentina. J. Geophys. Res. Earth Surf. 118, 1400–1418. https://doi.org/10.1002/jgrf.20102.

Habersack, H.M., 1996. Lack and surplus of sediments being transported by river systems. In: Walling, D.E., Webb, B.W. (Eds.), Erosion and Sediment Yield: Global and Regional Perspectives, Exeter, UK, pp. 565–573.

Habersack, H.M., Nachtnebel, H.P., 2005. Short-term effects of local river restoration on morphology, flow field, substrate and biota. Regul. Rivers Res. Manag. 10, 291–301. https://doi.org/10.1002/rrr.3450100222.

Habersack, H., Hein, H., Stanica, A., Liska, I., Mair, R., Jager, E., Hauer, C., Bradley, C., 2016. Challenges of river basin management: current status of, and prospects for, the river Danube from a river engineering perspective. Sci. Total Environ. 543, 828–845. https://doi.org/10.1016/j.scitotenv.2015.10.123.

Hardy, R.J., Best, J.L., Lane, S.N., Carbonneau, P.E., 2009. Coherent flow structures in a depth-limited flow over a gravel surface: the role of near-bed turbulence and influence of Reynolds number. J. Geophys. Res. Earth Surf. 114 https://doi.org/10.1029/2007JF000970.

Havinga, H., 2020. Towards sustainable river management of the Dutch Rhine River. Water 12, 1827. https://doi.org/10.3390/w12061827.

Havinga, H., Schielen, R.M.J., Van Vuren, S., 2009. Tension between navigation, maintenance and safety calls for an integrated planning of flood protection measures. In: Vionnet, C., García, M., Latrubesse, E., Perillo, G. (Eds.), River, Coastal and Estuarine Morphodynamics. RCEM2009, pp. 137–143.

Hegnauer, M., Beersma, J.J., Van den Boogaard, H.F.P., Buishand, T.A., Passchier, R.H., 2014. Generator of Rainfall and Discharge Extremes (GRADE) for the Rhine and Meuse Basins. Technical Report. Deltares, Delft, The Netherlands.

Hiemstra, K., van Vuren, S., Vinke, F., Jorissen, R., Kok, M., 2020. Assessment of the functional performance of lowland river systems subjected to climate change and large-scale morphological trends. Int. J. River Basin Manag. 1–12 https://doi.org/10.1080/15715124.2020.1790580.

Hohensinner, S., Habersack, H., Jungwirth, M., Zauner, G., 2004. Reconstruction of the characteristics of a natural alluvial river-floodplain system and hydromorphological changes following human modifications: the Danube River (1812–1991). River Res. Appl. 20, 25–41. https://doi.org/10.1002/rra.719.

Howard, A.D., 1982. Equilibrium and time scales in geomorphology: application to sand-bed alluvial streams. Earth Surf. Process. Landf. 7, 303–325. https://doi.org/10.1002/esp.3290070403.

Jansen, P., Van Bendegom, L., Van den Berg, J., De Vries, M., Zanen, A., 1979. Principles of River Engineering: The Non-tidal Alluvial River. Pitman, London.

Julien, P.Y., Klaassen, G.J., Ten Brinke, W.B.M., Wilbers, A.W.E., 2002. Case study: bed resistance of Rhine river during 1998 flood. J. Hydraul. Eng. 128, 1042–1050. https://doi.org/10.1061/(asce)0733-9429(2002)128:12(1042).

Kalweit, H., Buck, W., Felkel, K., Gerhard, H., 1993. Der Rhein unter der Einwirkung des Menschen: Ausbau, Schiffahrt, Wasserwirtschaft. Technical Report. Lelystad, KHR/CHR.

Keylock, C.J., Singh, A., Foufoula-Georgiou, E., 2014. The complexity of gravel bed river topography examined with gradual wavelet reconstruction. J. Geophys. Res. Earth Surf. 119, 682–700. https://doi.org/10.1002/2013JF002999.

Kirby, J.F., Swain, C.J., 2013. Power spectral estimates using two-dimensional morlet-fan wavelets with emphasis on the long wavelengths: jackknife errors, bandwidth resolution and orthogonality properties. Geophys. J. Int. 194, 78–99. https://doi.org/10.1093/gji/ggt103.

Lane, E.W., 1955. The importance of fluvial morphology in hydraulic engineering. Proc. Am. Soc. Civ. Eng. 81, 1–17.

Mackin, J.H., 1948. Concept of the graded river. Geol. Soc. Am. Bull. 59, 463–512. https://doi.org/10.1130/0016-7606(1948)59[463:Cotgr]2.0.Co;2.

Nicolleau, F., Vassilicos, J.C., 1999. Wavelets for the study of intermittency and its topology. Philos. Trans. R. Soc. Lond. 357, 2439–2457. https://doi.org/10.1098/rsta.1999.0441.

Nittrouer, J.A., Viparelli, E., 2014. Sand as a stable and sustainable resource for nourishing the Mississippi River delta. Nat. Geosci. 7, 350–354. https://doi.org/10.1038/ngeo2142.

Rijke, J., van Herk, S., Zevenbergen, C., Ashley, R., 2012. Room for the river: delivering integrated river basin management in the Netherlands. Int. J. River Basin Manag. 10 https://doi.org/10.1080/15715124.2012.739173.

Rijkswaterstaat, 2009. Nederlandse normen voor hydrografische opnemingen. Technical Report. Rijkswaterstaat, Lelystad, The Netherlands.

Riquier, J., Piégay, H., Michalkova, M.S., 2015. Hydromorphological conditions in eighteen restored floodplain channels of a large river: linking patterns to processes. Freshw. Biol. 60, 1085–1103. https://doi.org/10.1111/fwb.12411.

Sieben, A., 2009. Sediment management in the Dutch Rhine branches. Int. J. River Basin Manag. 17, 43–53. https://doi.org/10.1080/15715124.2009.9635369.

Simons, J.H.E.J., Bakker, C., Schropp, M.H.I., Jans, L.H., Kok, F.R., Grift, R.E., 2001. Man-made secondary channels along the river Rhine (The Netherlands); results of post-project monitoring. Regul. Rivers Res. Manag. 17, 473–491. https://doi.org/10.1002/rrr.661.

Surian, N., Rinaldi, M., 2003. Morphological response to river engineering and management in alluvial channels in Italy. Geomorphology 50, 307–326. https://doi.org/10.1016/s0169-555x(02)00219-2.

Ten Brinke, W.B.M., 1997. De bodemsamenstelling van Waal en IJssel in de jaren 1966, 1976, 1984 en 1995. Technical Report. Rijkswaterstaat Report 97.009. Arnhem, The Netherlands.

Ten Brinke, W.B.M., 2005. The Dutch Rhine: A Restrained River. Veen Magazines, Diemen, the Netherlands.

Torrence, C., Compo, G.P., 1998. A practical guide to wavelet analysis. Bull. Am. Meteorol. Soc. 79, 61–78. https://doi.org/10.1175/1520-0477(1998)079<0061:APGTWA>2.0.CO;2.

Van Denderen, R.P., Schielen, R.M.J., Straatsma, M.W., Kleinhans, M.G., Hulscher, S.J.M.H., 2019a. A characterization of side channel development. River Res. Appl. 35, 1597–1603. https://doi.org/10.1002/rra.3462.

Van Denderen, R.P., Schielen, R.M.J., Westerhof, S.G., Quartel, S., Hulscher, S.J.M.H., 2019b. Explaining artificial side channel dynamics using data analysis and model calculations. Geomorphology 327, 93–110. https://doi.org/10.1016/j.geomorph.2018.10.016.

Van Denderen, R.P., Kater, E., Jans, L.H., Schielen, R.M.J., 2022. Replication Dataset: Disentangling Changes in the River Bed Profile. 4TU.Centre for Research Data. https://doi.org/10.4121/19447043.

Van der Klis, H., 2003. Uncertainty Analysis Applied to Numerical Models of River Bed Morphology. Delft University of Technology, Delft, The Netherlands. PhD thesis.

Van Stokkom, H.T.C., Smits, A.J.M., Leuven, R.E.S.W., 2005. Flood defense in the Netherlands: a new era, a new approach. Water Int. 30, 76–87. https://doi.org/10.1080/02508060508691839.

Van Til, K., 1979. De Rijntakken van de bovenrivieren sedert 1600. Technical Report. Ministerie van Verkeer en Waterstaat, Rijkswaterstaat, Directie Bovenrivieren, Arnhem.

Van Vuren, S., Paarlberg, A., Havinga, H., 2015. The aftermath of "Room for the River" and restoration works: coping with excessive maintenance dredging. J. Hydro Environ. Res. 9, 172–186. https://doi.org/10.1016/j.jher.2015.02.001.

Vermeulen, B., Hoitink, A.J.F., Zolezzi, G., Abad, J.D., Aalto, R., 2016. Multiscale structure of meanders. Geophys. Res. Lett. 43, 3288–3297. https://doi.org/10.1002/2016GL068238.

Visser, P.J., 2000. Bodemontwikkeling Rijnsysteem: Een verkenning van omvang, oorzaken, toekomstige ontwikkelingen en mogelijke maatregelen. Technical Report. Delft University of Technology, Delft, the Netherlands.

Wilbers, A.W.E., 2002. The Development and Hydraulic Roughness of River Dunes. University of Utrecht. PhD thesis.

Wilbers, A.W.E., Ten Brinke, W.B.M., 2003. The response of subaqueous dunes to floods in sand and gravel bed reaches of the dutch Rhine. Sedimentology 50, 1013–1034. https://doi.org/10.1046/j.1365-3091.2003.00585.x.

Wohl, E., Lane, S.N., Wilcox, A.C., 2015. The science and practice of river restoration. Water Resour. Res. 51, 5974–5997. https://doi.org/10.1002/2014wr016874.

Wong, M., Parker, G., 2006. One-dimensional modeling of bed evolution in a gravel bed river subject to a cycled flood hydrograph. J. Geophys. Res. Earth Surf. 111 https://doi.org/10.1029/2006jf000478.

Ylla Arbós, C., Blom, A., Van Vuren, S., Schielen, R.M.J., 2019. Bed Level Change in the Upper Rhine Delta Since 1926 and Rough Extrapolation to 2050. Technical Report. Delft University of Technology, Delft.

Ylla Arbós, C., Blom, A., Viparelli, E., Reneerkens, M., Frings, R.M., Schielen, R.M.J., 2021. River response to anthropogenic modification: channel steepening and gravel front fading in an incising river. Geophys. Res. Lett. 48, e2020GL091338 https://doi.org/10.1029/2020GL091338.

Yuan, Y., Wei, H., Zhao, L., Cao, Y., 2009. Implications of intermittent turbulent bursts for sediment resuspension in a coastal bottom boundary layer: a field study in the western yellow sea, China. Mar. Geol. 263, 87–96. https://doi.org/10.1016/j.margeo.2009.03.023.